

Behaviour of a high-performance self-compacting concrete (HPSCC) with ternary mixtures of nano- and microsilica in the presence of chlorides

E. Reyes^a✉, J. Massana^b, F. Alonso^b, N. León^a, A. Moragues^a

a. Dpto. Ingeniería Civil, Construcción, Escuela Técnica Superior de Ingenieros de Caminos, Canales y Puertos, Universidad Politécnica de Madrid, (Madrid, Spain)
b. Dpto. de Ingeniería Agroforestal, Escuela Técnica Superior de Ingeniería Agronómica, Alimentaria y Biosistemas. Universidad Politécnica de Madrid, (Madrid, Spain)

✉ encarnacion.reyes@upm.es

Received 30 July 2019
Accepted 21 January 2020
Available on line 18 May 2020

ABSTRACT: In this paper, the influence of additions of nanosilica (nSi) and microsilica (mSi) on the behaviour of binary and ternary mixtures in chloride environments is studied. The main objective is to obtain high-performance self-compacting concrete (HPSCC) with a high durability which can meet specific demands in such aggressive environments. Ten blends were manufactured using Portland cement (CEM I 52.5 R) and additions of nSi and mSi in binary and ternary mixtures. The results of three tests frequently used to evaluate resistance to chloride penetration— electrical resistivity, migration and chloride diffusion —were studied and compared. Both binary and ternary mixtures presented significant improvements in chloride resistance, generally in proportion to the total content of the addition. In all the ternary mixtures, high resistivity is obtained, which indicates that such mixtures have a notably low chloride penetrability. Furthermore, these mixtures provided extremely low chloride diffusion coefficients even at small addition ratios.

KEYWORDS: High-performance concrete; Active addition; Durability; Diffusion; Corrosion.

Citation/Citar como: Reyes, E.; Massana, J.; León, N.; Moragues, A. (2020) Behaviour of a high-performance self-compacting concrete (HPSCC) with ternary mixtures of nano- and microsilica in the presence of chlorides. *Mater. Construcc.* 70 [339], e221 <https://doi.org/10.3989/mc.2020.10619>

RESUMEN: *Comportamiento frente a cloruros de un hormigón autocompactable de alta resistencia con mezclas ternarias de nano y micro sílice.* En este artículo se estudia la influencia en el comportamiento frente a cloruros de la adición de nanosílice (nSi) y microsílice (mSi) en mezclas binarias y ternarias. El principal objetivo es obtener un hormigón autocompactante de altas prestaciones con una alta durabilidad frente a estos ambientes agresivos con cloruros. Se prepararon diez dosificaciones usando cemento Portland (CEM I 52.5 R) y adiciones de nSi y mSi en mezclas binarias y ternarias. Se estudiaron y analizaron tres ensayos frecuentemente utilizados para evaluar la resistencia a la penetración de cloruros, resistividad eléctrica, migración y difusión de cloruros. Tanto las mezclas binarias como ternarias presentaron mejoras significativas en la resistencia a cloruros, en general proporcional al contenido de adición. En todas las mezclas ternarias se ha obtenido alta resistividad, indicando una penetrabilidad a cloruros notablemente baja. Estas mezclas proporcionaron un coeficiente de difusión de cloruros extremadamente bajo, incluso para bajos contenidos de adición.

PALABRAS CLAVE: Hormigón de altas prestaciones; Adición activa; Durabilidad; Difusión; Corrosión.

ORCID ID: E. Reyes (<https://orcid.org/0000-0002-1284-7335>); J. Massana (<https://orcid.org/0000-0003-2960-0491>); F. Alonso (<https://orcid.org/0000-0002-5095-385X>); N. León (<https://orcid.org/0000-0001-6427-798X>); A. Moragues (<https://orcid.org/0000-0001-7819-3066>).

Copyright: © 2020 CSIC. This is an open-access article distributed under the terms of the Creative Commons Attribution 4.0 International (CC BY 4.0) License.

1. INTRODUCTION

Many studies have been carried out on self-compacting concrete (SCC) (1–11). This type of concrete is mainly used to aid in proper formwork placement, particularly for formwork with complex shapes, and in structural elements with strongly reinforced sections in which the vibration process is complex and might move reinforcements. Simultaneously, SCC mitigates some operator health risks. The mixture dosage is designed to achieve a high degree of flowability that enables good consolidation through the action of the concrete's own weight without exudation or segregation (12, 13). Due to this property, SCC use has increased in construction and building, as well as in the pre-fabricated concrete industry, where the absence of vibration reduces production costs and increases the service life of moulds.

The advantageous workability and cohesion of SCC are mainly due to a high content in fines, a reduction in the content and size of coarse aggregates and the action of superplasticizer additives that provide the necessary flowability for casting work (13). Nepomuceno et al. (14) carried out a comprehensive study to correlate fresh and hardened properties of different mineral additions in binary blends, and they proposed a methodology for designing SCC mixtures. Various methods have been studied for designing a self-compacting mixture, depending on the properties required; a number of methods were recently examined by Shi, Wu, Lv and Wu (2015) (15). When an SCC has a high compressive strength and high durability, it is designed as a high-performance self-compacting concrete. HPSCC is generally prepared with a high cement content, from 400 to 600 kg/m³ (13), and a low water/cement ratio, which can be improved with the use of inactive additions (particularly limestone powder used as a filler (16, 17)) or active additions. Some case examples of the latter type are fly ash (18), blast furnace slag (19), microsilica (17, 18) and nanosilica (18, 20).

Significant strides have been made in the last two decades in improving the mechanical and resistant performance of concrete, particularly its compressive strength. Therefore, high- and ultra-high-strength concretes are relatively easily obtained now. However, making the mixture self-compacting and producing high-durability concrete for applications that require a service life of over 100 years is considerably more difficult. The main weakness in concrete durability involves the connectivity and size of the porous network, which determines the ingress of external aggressive substances that can affect the cement matrix and the steel embedded in the structural concrete. Prominent among these aggressive agents are chlorides. When chlorides reach the steel, they cause depassivation and corrosion, two

frequent mechanisms of degradation in the structural elements of reinforced concrete. Therefore, when the microstructure of cement-based materials becomes denser and has a refined porous network, it becomes more resistant to aggressive agents in general and chlorides in particular.

Conventionally, pozzolanic additions have been used to densify, reduce and refine the porous structure, due to the combined effect of the pozzolanic reactions and the filling effect associated with the small size of the material. Among the most interesting pozzolanic additions is microsilica (mSi), whose incorporation in cement-based mixtures has resulted in sound performance (21). However, the increase in structure service life currently demanded by sustainability-oriented technical requirements calls for cementitious materials with significant improvements in durability. For this reason, the influence of nanosilica (nSi) additions on concrete durability has been recently examined, since a greater, faster activity can be expected because of the significant increase of specific surface due to the small size of the nanoparticles. The study by Björnstrom et al. (2004) (22) showed that colloidal nanosilica has beneficial accelerating effects for the formation of hydrated products in cement. Some research has concluded that nanometric silica exhibits notable pozzolanic activity, increasing the formation of C-S-H gels, due to the secondary C-S-H generated by the reaction between portlandite and pozzolans (23, 24). Rong et al. (2015) (25) studied the influence of nanosilica additions on the mechanical performance, hydration process and microstructure evolution of ultra-high-performance cementitious composites. Their results showed that mechanical properties improved with the increase of the nanosilica content up to 3%, combined with a more homogenous, denser microstructure and acceleration of the hydration process, which was mainly attributed to the pozzolanic and filler effects of nanosilica. A review of nanosilica's contribution to the mechanical and durability properties of cement-based materials can be consulted in Balapour et al. (26). These nanoparticles can also facilitate the nucleation of hydrated cement crystals, generating changes not only in the rate of hydration, but also in the morphology and size of the hydrated compounds (17). However, the use of nSi presents considerable technical difficulties, such as a high water demand, which makes the mixing operation problematic (even more so in the case of SCC). Therefore, identifying improvements is not as simple as it might appear. Numerous published authors have compared the behaviour of nano- and microsilica (nSi and mSi) additions. Jalal et al. (18) studied the influence of these additions on the mechanical properties, water absorption, electrical resistivity and chloride ion penetration of binary and ternary HPSCC mixtures and found that the refinement of the microstructure obtained using nSi

and mSi could improve strength and durability properties, particularly at greater ages. Gesoglu et al. (27) focused on the effect of using nSi and mSi in binary and ternary blends on the mechanical properties of low-binder, ultra-high performance cementitious composites. The results obtained with mixtures containing nSi and mSi showed better mechanical behaviour than binary mixtures. Similarly, in previous work (28) the authors examined the fresh and mechanical behaviour of binary and ternary mixtures of HPSCC. Ternary mixtures showed better fresh behaviour than binary mixtures containing the same total amount of additions. Furthermore, these ternary mixtures present the best mechanical behaviour. However, there are few published works that evaluate the effects of nSi, mSi and ternary combinations on the durability properties of HPSCC, such as freeze-thaw and carbonation-process resistance, which are very important for concrete structures in some aggressive environments (25, 29). For example, freeze-thaw resistance is considered fundamental for both precast and on-site structural elements used in natural environments with frequent frost action, such as high-mountain environments.

HPSCC seems to be a promising material for many applications and structures. However, its performance must be studied before it is widely adopted in construction. Also, the behaviour of structural elements made with HPSCC has to be more thoroughly understood, and design provisions in step with the latest advances are needed. This paper forms part of a larger research effort into the influence of binary and ternary mixtures of mSi and nSi in different proportions on the properties of fresh and hardened-state HPSCC (28, 29). Designing self-compacting mixtures with these additions is a challenge, due to the notable loss of workability they cause. Adequate SCC flowability was achieved in this study due to chemical additives compatible with the mixture in suitable proportions. Although there are some studies of the behaviour of SCC in resisting chlorides (30), there is a lack of published research about the durability of SCC in chloride-rich environments, despite the increase of its use. In this paper, the chloride resistance of HPSCC prepared with binary and ternary mixtures using mSi and nSi is studied at the reference age of 28 days. In these mixtures, the effect of greater compactness due to the increased packing density derived from

using nano- and micrometric additions together is combined with the enhancement of reactivity derived from increased specific surface. The main objective is to obtain HPSCC with notably high durability which can respond to specific demands. As previously mentioned, further knowledge of how a concrete behaves when attacked by chlorides is one of the fundamental aspects in determining concrete durability (1, 2). This work provides the results of three tests frequently used to assess resistance to chloride penetration: electrical resistivity (3–10), chloride migration and chloride diffusion. The model described in EHE (13) is used to estimate the service life of the structure from the values of the chloride diffusion coefficient. Analysis and comparison of the results obtained from the HPSCC mixtures allow the study to find optimised dosages for the fabrication of high-sustainability structural elements in chloride-rich environments.

2. EXPERIMENTAL STUDY

2.1. Materials used and mixture proportioning

In this study, 10 blends were designed (31) for obtaining HPSCC with CEM I 52.5 R (PC) cement and two mineral admixtures, nSi and mSi, in different percentages in reference to cement weight. Table 1 presents the chemical composition and physical properties of the cementitious materials used. The nSi was dispersed in water, under the trade name of Levasil® 200/40%, with 40% solids by weight, a specific surface area of $200 \text{ m}^2\text{g}^{-1}$ and a particle size of approximately 15 nm (see Table 1). The mSi used was Elkem Microsilica® MS 940 U, a material composed of nonporous amorphous spheres of SiO_2 with submicron size and small agglomerates, with a specific surface area of $15\text{--}30 \text{ m}^2\text{g}^{-1}$ and a particle size of approximately 0.15 micron (see Table 1). Even when some of the spheres may be found separately, the majority tend to form agglomerates of primary particles with a size range from 0.1 to 1.0 micron. Additions (nSi and mSi) were not used as a cement replacement, but as an additional cementitious material.

The aggregates and proportioning used in the mixtures were as follows: 1160 kg/m^3 of siliceous sand (termed A) measuring less than 4 mm in diameter, with a fineness modulus of 3.30; 585 kg/m^3

TABLE 1. Properties of Portland cement (PC) and mineral additions (nSi, mSi).

	SiO ₂	Al ₂ O ₃	Fe ₂ O ₃	CaO	MgO	SO ₃	K ₂ O	Na ₂ O	Loss on ignition (%)	Density (g·cm ⁻³)	Specific surface area (m ² ·g ⁻¹)
PC	19.20	6.07	1.70	63.41	2.56	3.38	0.2	0.33	2.09	3.5	0.42
nSi	99.90	-	-	-	-	-	-	-	0.10	1.29	200
mSi	94	-	-	-	-	-	-	-	-	0.7	30

of rolled gravel (G) measuring 6 mm to 12 mm in diameter; and 100 kg/m³ of limestone filler (LF) with a granulometry in accordance with UNE 12620:2003+A1:2009 (32) and a maximum diameter of 63 µm. All the SCCs were prepared using a water-to-cementitious material ratio (w/cm) of 0.36 and 450 kg/m³ of cement.

Additionally, two chemical additives were used: SIKA ViscoCrete® 5720, based on polycarboxylate polymers (solids content 36%, density 1.09 kg/l), as superplasticizer (SP) and SIKA Stabilizer® 4R (solids content 3–3.5%, density 1.03 kg/l) as stabilizer (MV), which controls concrete viscosity with a constant amount in mixtures of 0.15% by weight of cement (wt.%).

Ten HPSCC dosages were designed. In order to obtain reference values to compare the results, an HPSCC without mineral additions was prepared (CEM I 52.5 R as the sole cementitious material), identified as HAC. Three dosages were made with 2.5%, 5% and 7.5% nSi, which were respectively identified as HAC[nSi]-2.5, HAC[nSi]-5 and HAC[nSi]-7.5. Three more were made with 2.5%, 5% and 7.5% mSi, which were identified as HAC[mSi]-2.5, HAC[mSi]-5 and HAC[mSi]-7.5. Lastly, the remaining three dosages were made by using admixtures of both nSi and mSi (ternary mixtures) in percentages, respectively, of 2.5%/2.5%, 5%/2.5% and 2.5%/5% (identified as HAC[nmSi]-2.5/2.5, HAC[nmSi]-5/2.5

and HAC[nmSi]-2.5/5). Table 2 shows the mixture proportions.

The tests performed on the blends to determine self-compacting were as follows: slump-flow diameter [d_f (mm)], V-funnel flow time [T_V (s)] and L-box height ratio [C_{bl}] (12, 13). The values obtained from the tests for all the mixes were within the range that guarantees self-compactability. Once hardened, compressive strength, tensile strength and modulus of elasticity were obtained to characterize the mechanical and resistant properties of all blends. Table 3 shows the fresh properties corresponding to self-compacting tests and the compressive strength at 28 days for all mixtures. Detailed information on the results is available in previously published works (28, 29).

2.2. Test programme

Pore-size distribution and total porosity were evaluated by Mercury Intrusion Porosimetry (MIP), according to ASTM D4404-84 (2004), using a Micromeritics Autopore IV 9500 at a maximum pressure of 33,000 psi, with a range of 5 nm to 180 µm.

For electrical resistivity tests, cylindrical moulds 200 mm long and 100 mm in diameter were used to prepare a total of 30 specimens (three specimens per dosage). Electrical resistivity was determined by a

TABLE 2. HPSCC mixture proportions.

Material (kg/m ³) (%)	HAC	HAC	HAC [nSi]-5	HAC [nSi]-7.5	HAC [mSi]-2.5	HAC [mSi]-5	HAC [mSi]-7.5	HAC [nmSi]-2.5/2.5	HAC [nmSi]-5/2.5	HAC [nmSi]-2.5/5
nSi	-	11.25	22.5	33.75	-	-	-	11.25	22.5	11.25
		2.5%	5%	7.5%				2.5%	5%	2.5%
mSi	-	-	-	-	11.25	22.5	33.75	11.25	11.25	22.5
					2.5%	5%	7.5%	2.5%	2.5%	5%
Water	162	166	170.1	174.1	166	170.1	174.1	170.1	174.1	174.1
SP (%)	2	3.30	4	6	2.30	2.50	2.70	3.60	4.80	3.90

TABLE 3. Results of self-compacting and compressive strength tests.

Self-compacting tests	HAC	HAC [nSi]-2.5	HAC [nSi]-5	HAC [nSi]-7.5	HAC [mSi]-2.5	HAC [mSi]-5	HAC [mSi]-7.5	HAC [nmSi]-2.5/2.5	HAC [nmSi]-5/2.5	HAC [nmSi]-2.5/5
Slump-flow diameter d_f (mm)	650	720	635	565	787	817	795	685	675	752
V-funnel flow time T_V (s)	8	11	13	17	10	7	5	12	12	10
L-box height ratio C_{bl}	0.98	0.96	0.81	0.85	0.95	0.95	1	0.89	0.97	0.97
Slump-flow class	SF1	SF2	SF1	SF1	SF3	SF3	SF3	SF2	SF2	SF2
Compressive strength (28 days) (MPa)	62.46	63.79	65.01	68.86	65.73	68.37	70.35	82.17	71.15	69.25

non-destructive test carried out under room conditions on samples saturated to constant weight. Mortars were tested at 7, 28 and 365 days to analyse their evolution over time after a 28-day curing process at room temperature ($20 \pm 2^\circ\text{C}$) and 95% relative humidity. This test was carried out according to UNE 83988-1 (33) using Giatec RCON equipment. Such equipment measures electrical resistance with frequencies from 1 to 30 kHz. Electrical resistivity was then calculated using Equation [1]. Each mixture's resistivity was calculated as the average value from three measurements.

$$\rho_e = K \cdot R_e \quad [1]$$

where:

ρ_e : electrical resistivity ($\Omega \text{ m}$)

K: cell constant (m)

R_e : electrical resistance (Ω)

The cell constant K is found by Equation [2]:

$$K = \frac{S}{L} \quad [2]$$

where:

K: cell constant (m)

S: surface area of the specimen through which the electrical charge passes (m^2)

L: specimen height (m)

The test entailed non-destructive testing and is an indirect measure of the connectivity and tortuosity parameters of concrete porosity, which have a significant influence on resistance against chloride penetration. The electrical resistivity value is related to chloride penetrability through the determination of the electrical charge (coulombs) that passes through a specimen in a determined time, as in ASTM C1202 (34). Table 4 shows the quality classification according to this value.

With the aim of analysing the evolution of the concretes' resistivity over time, the specimens were tested at the ages of 7, 28 and 365 days.

TABLE 4. Quality classification of concrete according to chloride penetrability.

Electrical charge that passes (coulombs) ASTM C1202	Electrical resistivity ($\Omega \text{ cm}$) UNE 83988-1	Chloride penetrability
> 4000	< 5	High
2000 to 4000	5 to 10	Moderate
1000 to 2000	10 to 20	Low
100 to 1000	20 to 200	Very low
< 100	> 200	Negligible

In order to determine the chloride migration coefficient, two slices 100 mm in diameter and 50 mm in length for each mixture were tested according to the NT BUILD 492 (1999) standard (35). These slices were taken from the central part of the cylindrical specimens (diameter 100 mm, height 200 mm) after 28 days of curing, prepared according to the standardised procedure and subjected to a difference in electric potential for a specified time. Each slice was then cracked axially by the indirect traction method with a press. Then a solution of silver nitrate 0.1 M was applied to the surface of the specimens, and the depth of chloride penetration was measured. The non-steady-state migration coefficient (D_{nssm}) is obtained by Equation [3]:

$$D_{\text{nssm}} = \frac{0.0239 (273+T) L}{(U-2) t} \left(X_d - 0.0238 \sqrt{\frac{(273+T) L X_d}{U-2}} \right) \quad [3]$$

where:

D_{nssm} : non-steady-state migration coefficient ($\times 10^{-12} \text{ m}^2/\text{s}$)

U: absolute value of the voltage applied (V)

T: average temperature of the anode solution between its initial and final value ($^\circ\text{C}$)

L: specimen thickness (mm)

X_d : average depth of chloride penetration (mm)

t: test duration (hours)

The chloride diffusion test was carried out according to the CEN/TS 12390-11 standard (36). The specimens were obtained from cutting the cylindrical specimens cured at 28 days and according to the standard procedure. All the cuts were made with the Struers Secotom-10 precision diamond cut-off machine, with a 0.8 mm-thick disc. Liquid petroleum jelly was used to cool the cutting disc without washing away the chlorides. Layers 2 mm thick were obtained. Then, these layers were ground to be analysed by a chemical procedure to determine chloride concentration by using a Metrohm model 916 Ti-Touch titrator. The total chloride concentration was measured according to the standard test method in UNE-EN 14629:2007 (37) at several depths to find the apparent chloride diffusion coefficient.

The test results yielded the surface chloride concentration on the exposed surface (% mass) (C_s) and the apparent diffusion coefficient (m^2/s) (D_a), obtained by fitting Equation [4] by means of a non-linear regression according to the least squares method.

$$C(x,t) = C_s - (C_s - C_i) \cdot \text{erf} \left(\frac{x}{\sqrt{4 \cdot D_a \cdot t}} \right) \quad [4]$$

where:

$C(x, t)$: total chloride concentration at depth x and time t (% mass)

C_i : initial chloride concentration (% mass)

x : depth from the exposed surface (m)

t : exposure time (s)

erf : error function defined in Equation [5]

$$erf(z) = \frac{2}{\sqrt{\pi}} \cdot \int_0^z \exp(-u^2) du \quad [5]$$

Once the apparent diffusion coefficient is obtained, the chloride penetration coefficient (K_{Cl}) is calculated following Equation [6] (13):

$$K_{Cl} = \alpha \cdot \sqrt{12 \cdot D_t \left(1 - \sqrt{\frac{C_{th} - C_b}{C_s - C_b}} \right)} \quad [6]$$

where:

α : unit conversion factor equal to 56157

D_t : apparent diffusion coefficient for time t expressed in cm^2/s

C_{th} : critical chloride concentration at which the passive barrier of steel is broken, in % of cement weight

C_s : chloride concentration on the surface of the concrete, expressed in % of cement weight

C_b : content of chloride from materials (initial chloride concentration)

The chloride penetration coefficient enables the corrosion initiation time to be predicted for a given concrete cover thickness according to Equation [7] (13):

$$t = \left(\frac{d}{K_{Cl}} \right)^2 \quad [7]$$

where:

t : corrosion initiation time in years

d : concrete cover thickness in mm

K_{Cl} : apparent chloride penetration factor in m/years

The free chloride concentration of the same concrete specimens was measured experimentally following the recommendations of RILEM TC 178-TMC (38). The free chloride concentration at several depths enabled the effective chloride diffusion coefficient to be obtained by following a procedure similar to that described for the apparent chloride diffusion coefficient. The bound concentration was determined by subtracting the free chloride concentration from the total concentration.

3. RESULTS AND DISCUSSION

3.1. Pore network

Table 5 shows the total porosity and the macro- and micropore percentages for all mixtures at 7 and 28 days. In this research, macropores are considered to be pores with a diameter larger than 50 nm in accordance with IUPAC 1984 (39).

As can be observed, the results show that the use of nSi and mSi may have a positive effect on improving the microstructure and reducing the internal pore structure at both ages and in all mixtures as compared to the reference mixture (HPSCC). It could be said that nSi causes a reduction in pore diameter, though it is associated with a slight decrease in total porosity. This effect might be explained by the formation of a larger amount of C-S-H gels and gel pores due to the high pozzolanic activity of the nSi addition in regard to its great surface/volume ratio, reducing pore size. In the case of mixtures with mSi, a significant reduction of total porosity is observed (which might be due to a filling effect of the addition), while pore size remains unchanged. When nSi and mSi additions are combined in ternary mixtures, an overlap of both effects is observed. In this case, the behaviour might be explained by an enhanced hydration process (due to the presence of the nSi addition) and the final packing efficiency (related to the continuity of the particle size distribution of the components).

3.2. Electrical resistivity

As explained above, in order to measure electrical resistivity, a voltage was applied between two electrodes, and the current transmitted through the water solution within the pores was measured. This method was used mainly to determine chloride penetrability. Polder in 2001 (40) described methods to assess concrete resistivity on site for various purposes related to reinforcement corrosion and protection. Polder discussed practical aspects, proposed guidelines for calibration and interpretation and gave reference values for several cases. Basheer et al. in 2002 (41) monitored the behaviour of concretes containing alternative cementitious materials (metakaolin, microsilica, pulverised fuel ash and ground granulated blast furnace slag) in a chloride exposure regime. For this purpose, they measured the changes in resistance between pairs of stainless steel electrodes embedded in the concrete at different depths from the exposed surface. The method provided useful information that could be related to the chloride diffusion characteristic of the different mixtures. Rajabipour et al. (42) proposed a method to interpret electrical conductivity measurements in concrete to assess water penetration. The procedure enables the position of moisture to be resolved, and

TABLE 5. Total porosity and percentage of macro- and micropore values for all mixtures.

		Total porosity (%)	Macropores ($\text{\O} > 50 \text{ nm}$)	Micropores ($\text{\O} < 50 \text{ nm}$)
HAC	7	9.24	24.02	75.98
	28	9.31	16.83	83.17
HAC[nSi]-2.5	7	9.91	23.49	76.51
	28	8.10	13.32	86.68
HAC[mSi]-5	7	9.03	8.60	91.40
	28	8.34	13.05	86.95
HAC[nSi]-7.5	7	9.98	8.49	91.51
	28	7.43	11.87	88.13
HAC[mSi]-2.5	7	9.00	15.31	84.69
	28	7.15	21.63	78.37
HAC[mSi]-5	7	9.09	15.07	84.93
	28	6.97	27.03	72.97
HAC[mSi]-7.5	7	8.36	18.88	81.12
	28	7.34	16.32	83.68
HAC[nmSi]-2.5/2.5	7	9.18	15.96	84.04
	28	7.36	21.40	78.60
HAC[nmSi]-5/2.5	7	9.65	10.87	89.13
	28	8.61	14.08	85.92
HAC[nmSi]-2.5/5	7	8.83	9.34	90.66
	28	7.13	12.73	87.27

it is significantly superior to previous approaches. McPolin et al. in 2005 (43) carried out an investigation to monitor the rate of ingress of chlorides in concrete with additions to mixtures. They obtained the chloride profiles and determined the resistivity of the concrete in order to assess if resistivity could be used to determine the presence of chlorides. The results of the resistivity profiles corresponded well with the chloride profiles. More recently, in 2014 Andrade et al. (44) developed an alternative model to calculate the service life of reinforced concrete based on electrical resistivity.

The average values of electrical resistivity at 7, 28 and 365 curing days for mixtures with nSi, mSi and ternary mixtures of nmSi are shown, respectively, in Figure 1, Figure 2 and Figure 3. All concretes with additions presented a significantly higher electrical resistivity than did the concrete without additions. An increase in resistivity was observed when the addition percentage was increased, both for binary and ternary mixtures, regardless of the type of addition. Among the mixtures with a higher addition content, the highest resistivity figures were obtained for the mixtures with 7.5% microsilica, and the lowest figures were found for the concrete with 7.5% nanosilica. However, in the case of the ternary mixtures, the mixture containing the highest amount of microsilica was not that which showed the highest

resistivity. The use of two sizes of additions may contribute to a better packing of the component particles of the material. The difficulty of compaction of mixtures with a high nanosilica content could explain the results.

In general, an increase in electrical resistivity was obtained with time. However, the resistivity values at 365 days of curing for the HAC[nSi]-7.5 and HAC[nmSi]-2.5/5 mixtures were lower than those obtained at 28 days. This may be due to a notably low capillary absorption of the mixtures containing a greater total amount of nanosilica addition, which would result in especially good chloride resistance.

It may also be observed that the addition of nanosilica produced a significant increase in resistivity at seven days of curing: up to 675.3% for the HAC[nSi]-7.5 mixture, in comparison with HAC alone. This result could be of significant importance in applications where low chloride penetrability at an early age is required. The percentages of increment decreased at later ages of curing, and the improvement lessened with a lower content of total addition. Even so, the smallest increase in resistivity was 42% for HAC[nSi]-2.5 at 365 days of curing.

In the case of mixtures with mSi, a significant increase in electrical resistivity from 7 to 28 days of curing was observed. The percentages of these increases in electrical resistivity with respect to the

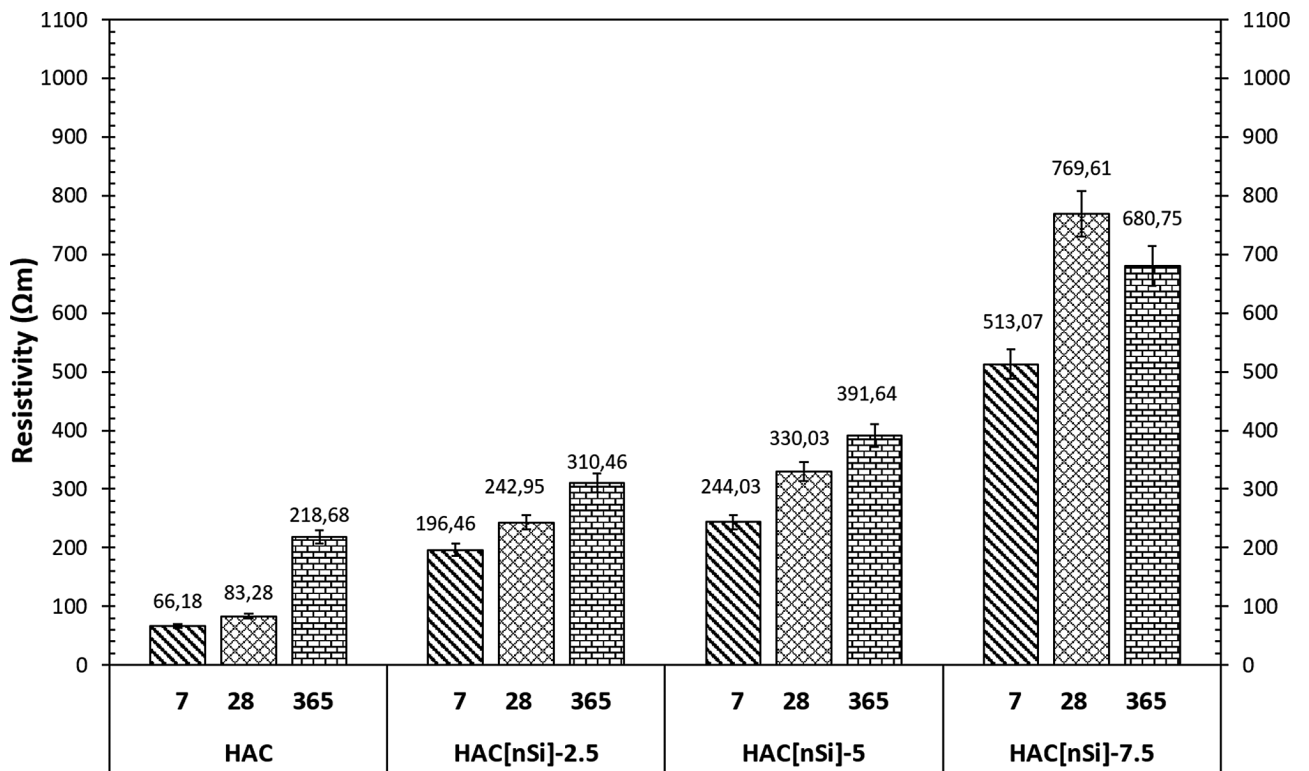


FIGURE 1. Average values and error bars of electrical resistivity at 7, 28 and 365 curing days for mixtures with nSi additions.

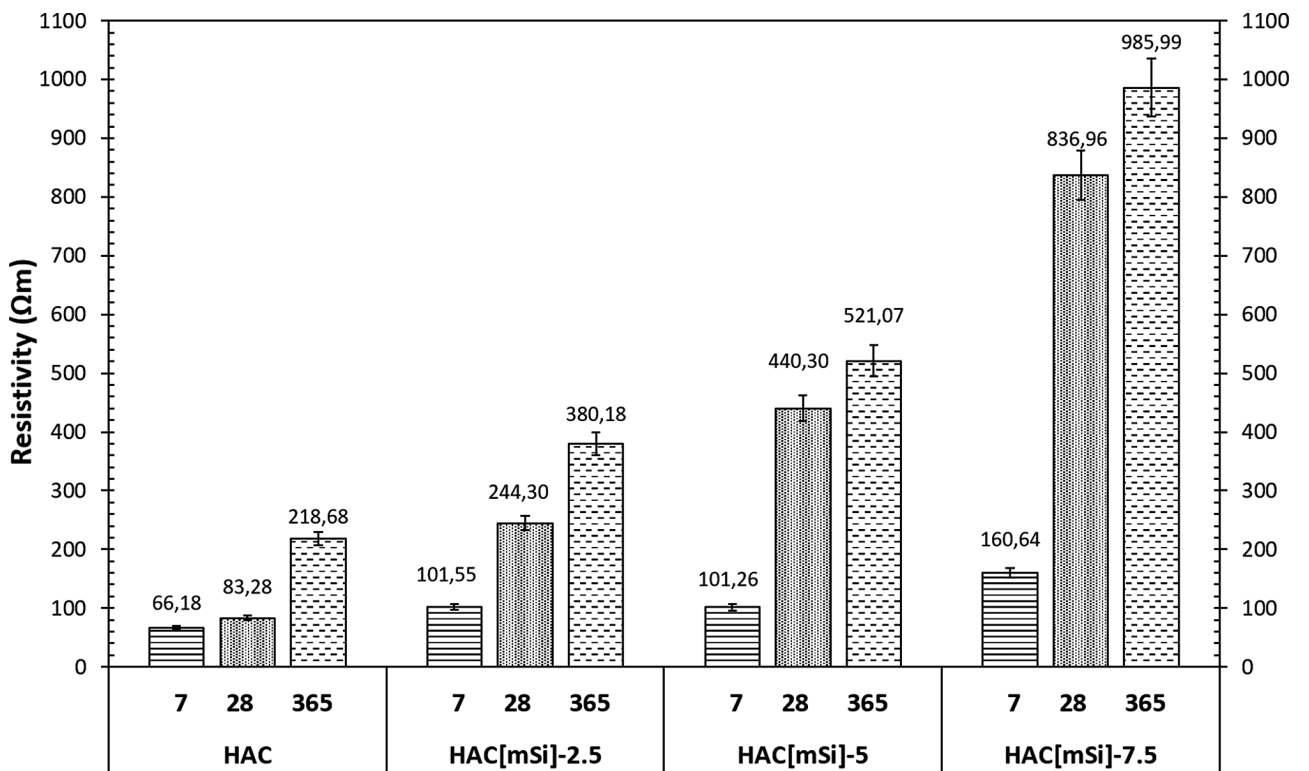


FIGURE 2. Average values and error bars of electrical resistivity at 7, 28 and 365 curing days for mixtures with mSi additions.

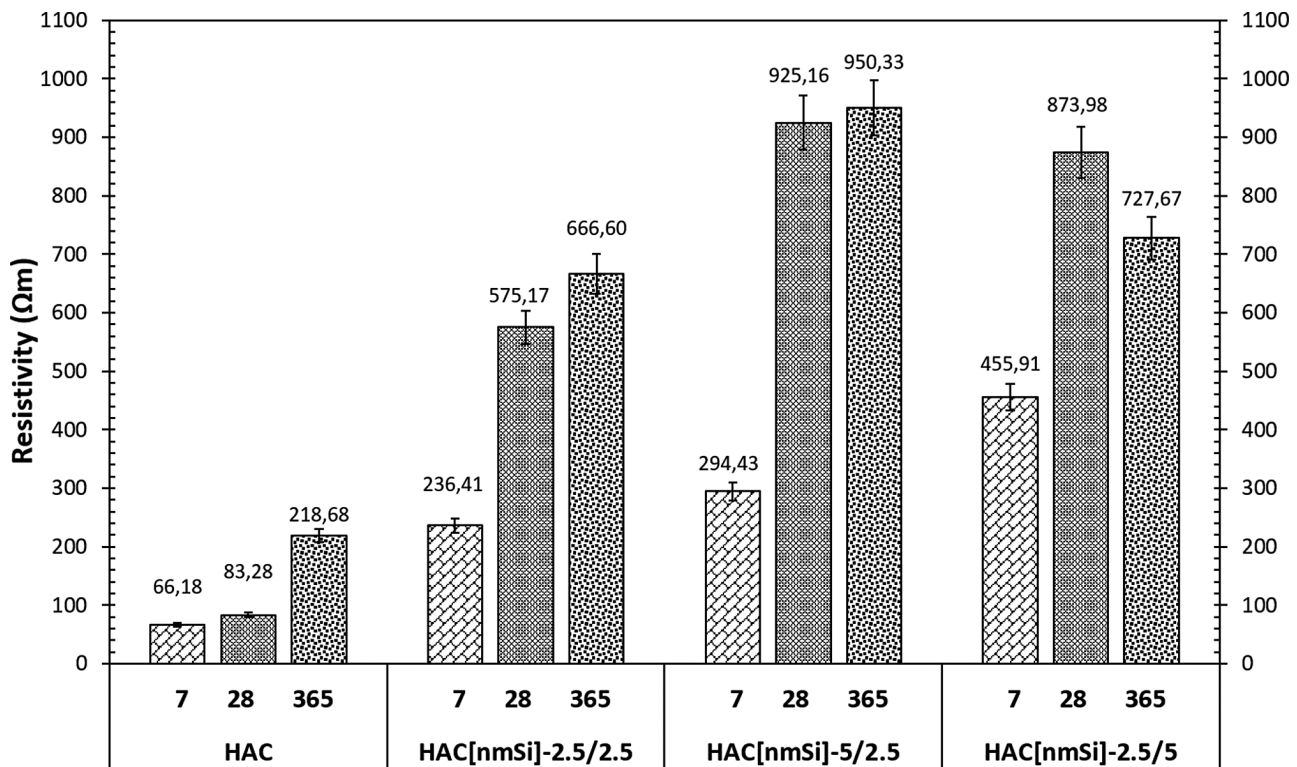


FIGURE 3. Average values and error bars of electrical resistivity at 7, 28 and 365 curing days for mixtures with ternary mixtures of nmSi.

reference range from 53.01% (HAC[mSi]-2.5) to 142.73% (HAC[mSi]-7.5) at seven days of curing and vary from 193.36% (HAC[mSi]-2.5) to 905% (HAC[mSi]-7.5) at 28 days.

Among the ternary mixtures, HAC[nmSi]-5/2.5 presented the highest electrical resistivity, with 925.16 Ωm after 28 days of curing. These concretes, like the binary mixtures with the addition of mSi, experienced the highest increase in their electrical resistivity from 7 to 28 days.

The improvement in resistivity behaviour achieved with nSi at seven days may be attributed to pore refinement, a reduction in the percentage of macropores due to the pozzolanic reaction and the packing effect observed at early ages. Binary mixtures with nSi showed a pore size reduction proportional to the amount of addition. In binary mixtures with mSi, the microstructure produced had a significantly lower total porosity at 28 days due to a slower pozzolanic reaction, reaching resistivity values similar to binary mixtures with nSi at this age. The average pore size of binary mixtures with mSi was similar to that of the reference concrete. Lastly, the ternary mixtures developed a microstructure that is a result of the combination of both effects, exhibiting a small average pore size (proportional to the amount of nSi) and a lower total porosity (proportional to

the amount of mSi). This may explain the resistivity results; the best values at both ages came from the ternary mixtures, possibly because of their having a continuous particle size distribution from the smallest particle size (addition) to the largest particle size (coarse aggregate) in the dosage of the mixture.

Table 6 shows the classification of chloride penetrability at 7, 28 and 365 days of curing, according to the ASTM C1202 standard (34). The reference concrete (HAC) ranges from moderate penetrability at 7 and 28 days to significantly low penetrability at 365 days of curing. The concretes with the nanosilica addition are classified as having a significantly low penetrability as of seven days of curing. Binary mixtures with microsilica exhibit low penetrability after seven days of curing and notably low penetrability after 28 days of curing. Lastly, ternary mixtures are classified as having an especially low penetrability as of seven days of curing.

Given these results, it is noteworthy that concretes with nanosilica are classified in the same level in both binary and ternary mixtures, providing notably low chloride penetrability from early ages.

It is also important to mention that the classification places all concretes, including the reference concrete, in the same category at 365 days. Therefore, if only this category were considered, the use of

TABLE 6. Classification of chloride penetrability at 7, 28 and 365 days of curing, according to the ASTM C1202 standard.

Mixtures	HAC	HAC [nSi]-2.5	HAC [nSi]-5	HAC [nSi]-7.5	HAC [mSi]-2.5	HAC [mSi]-5	HAC [mSi]-7.5	HAC [nmSi]-2.5/2.5	HAC [nmSi]-5/2.5	HAC [nmSi]-2.5/5
Resistivity (kΩ cm) (7 days)	6.62	19.65	24.40	51.31	10.15	10.13	16.06	23.64	29.44	45.59
Chloride penetrability (7 days)	Moderate	Very low	Very low	Very low	Low	Low	Low	Very low	Very low	Very low
Resistivity (kΩ cm) (28 days)	8.33	24.30	33.00	76.96	24.43	44.03	83.70	57.52	92.52	87.40
Chloride penetrability (28 days)	Moderate	Very low	Very low	Very low	Very low	Very low	Very low	Very low	Very low	Very low
Resistivity (kΩ cm) (365 days)	21.87	31.05	39.16	68.07	38.02	52.11	98.60	66.66	95.03	72.77
Chloride penetrability (365 days)	Very low	Very low	Very low	Very low	Very low	Very low	Very low	Very low	Very low	Very low

different additions would seem irrelevant after one year. This is because the classification establishes a rather wide range for the real values of resistivity in each category and assigns chloride penetrability levels on the sole basis of whether the value lies within this wide range. This should be noted, since concretes that differ by as much as 350% in electrical resistivity (as is the case of HAC[mSi]-7.5 in comparison with the reference concrete) lie within the same category. In addition, this classification does not allow the service life of a concrete to be estimated.

3.3. Chloride migration coefficient

Ion transport in mortar specimens was evaluated through chloride migration tests according to the NT BUILD 492 standard (18), which enabled the non-steady-state migration coefficient (D_{nssm}) to be obtained.

Figure 4, Figure 5, and Figure 6 show the average values of the chloride migration coefficient for three specimens containing mixtures with nSi and mSi and ternary mixtures of nmSi, respectively, compared with HAC, all at 28 curing days.

As can be observed in Figure 4, the chloride migration coefficient decreases significantly in comparison with the reference with the increase in the nanosilica content. The values vary from 43.11% for HAC[nSi]-2.5 to 87.91% for HAC[nSi]-7.5. The chloride migration coefficient for the reference concrete is $6.29 \times 10^{-12} \text{ m}^2/\text{s}$. Since this lies below $10 \times 10^{-12} \text{ m}^2/\text{s}$, the concrete is considered notably resistant to chloride penetration. A chloride migration coefficient below this reference value means the estimated service life of the concrete is high. Therefore, reducing the coefficient to values such as $0.76 \times 10^{-12} \text{ m}^2/\text{s}$ might represent a significant increase in the useful life of concrete structures.

In Figure 5 a significant decrease can be observed with the increase of the content of addition. The decrease was 85.89% for HAC[mSi]-7.5. The coefficient in this type of concrete presented lower values than in concretes with nanosilica, except for HAC[mSi]-7.5, which has a slightly higher coefficient (16.73%) than HAC[nSi]-7.5.

Figure 6 shows that ternary specimens had values of under $1 \times 10^{-12} \text{ m}^2/\text{s}$ in all cases. In the case of HAC[nmSi]-2.5/2.5, with 5% total addition, the chloride migration coefficient was similar to that obtained with 7.5% of either addition separately. The percentages of decrease of the chloride migration coefficient in these concretes are 84.45% for HAC[nmSi]-2.5/2.5, 90.42% for HAC[nmSi]-5/2.5 and 89.50% for HAC[nmSi]-2.5/5, in comparison with the reference concrete HAC. When comparing ternary mixtures with a 7.5% total addition content, a slightly lower chloride migration coefficient was obtained with the higher percentage of nanosilica addition, HAC[nmSi]-5/2.5.

To study how the amount of addition influences the chloride migration coefficient, three regression curves have been calculated, one for each type of concrete with additions (see Figure 7). Here a good fit may be observed by means of an exponential regression with an R^2 of 0.995 for concrete with nSi, 0.981 for concrete with mSi and 0.976 for concrete with both additions. Binary and ternary mixtures follow similar trends, indicating that the effectiveness of silica against migration depends mainly on its pozzolanic activity. Results are similar for the same amount of total addition, depending only slightly on particle size. As the amount of total addition increases, the chloride migration coefficient tends to present similar values. This may be observed in the case of all concretes with the 7.5% addition: their values range from $0.60 \cdot 10^{-12} \text{ m}^2/\text{s}$ for HAC[nmSi]-5/2.5 to $0.89 \cdot 10^{-12} \text{ m}^2/\text{s}$ for HAC[mSi]-7.5 and thus are close to overlapping.

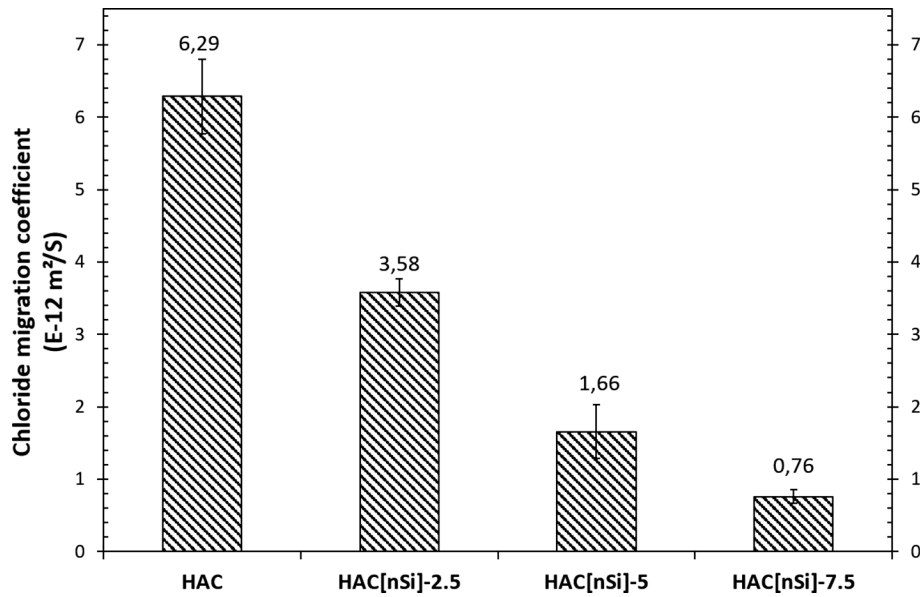


FIGURE 4. Average values and error bars of chloride migration coefficient at 28 curing days for mixtures with nSi compared with HAC.

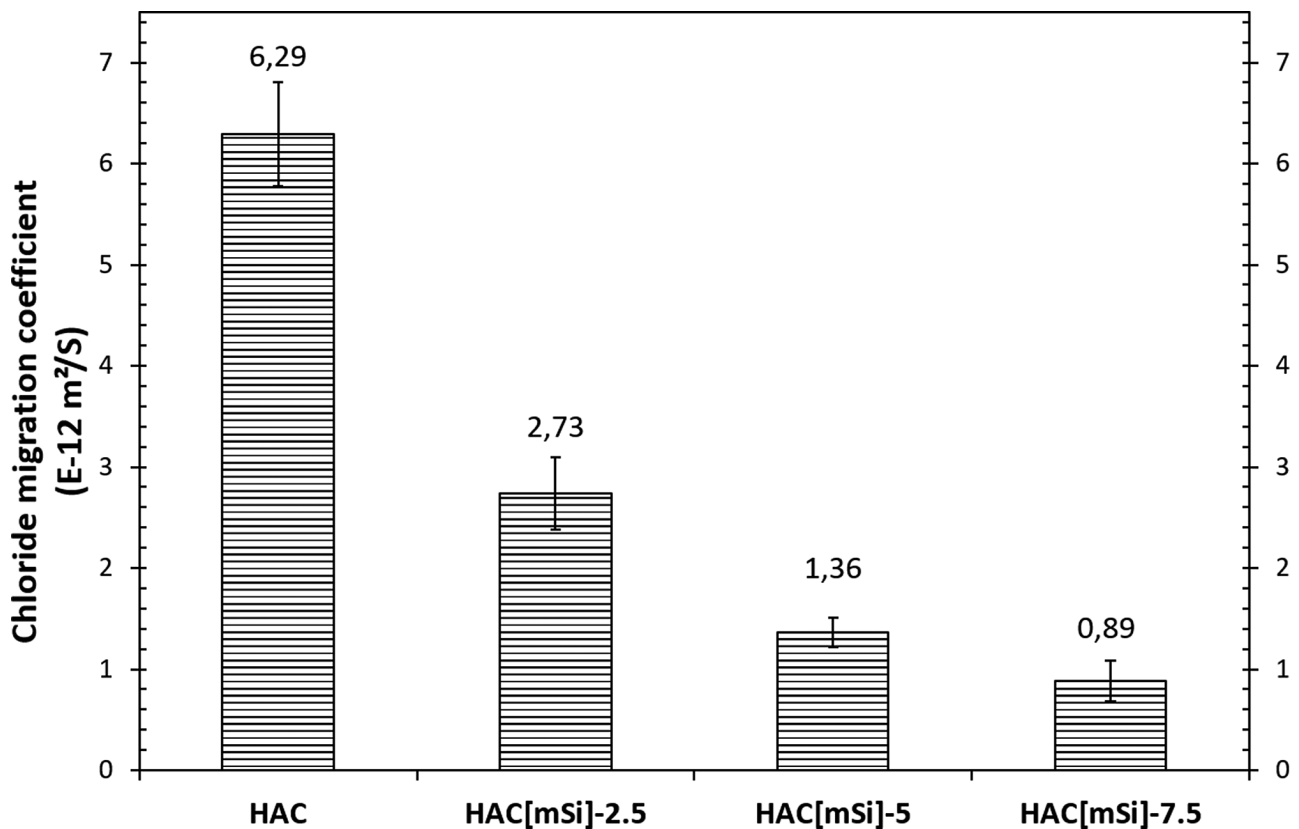


FIGURE 5. Average values and error bars of chloride migration coefficient at 28 curing days for mixtures with mSi compared with HAC.

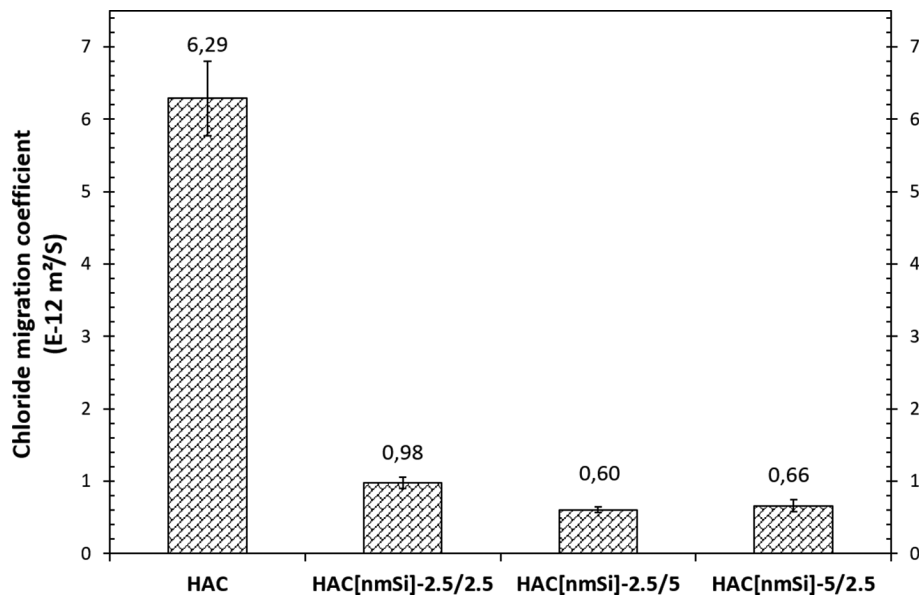


FIGURE 6. Average values and error bars of chloride migration coefficient at 28 curing days for mixtures with ternary mixtures of nmSi compared with HAC.

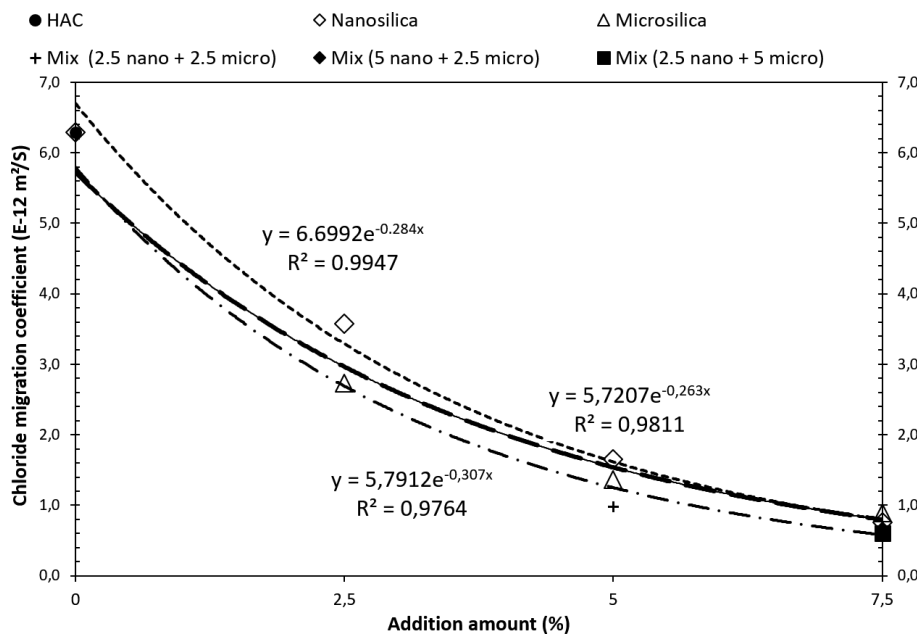


FIGURE 7. Regression curves of the influence of addition amount on the chloride migration coefficient.

Given the results, the use of addition provides HPSCC with good resistance against chloride migration, as the published literature has shown (45–47). However, reducing the coefficient from 43% to 50% by using a 2.5% addition, as shown in this work, represents a significant improvement. This enhanced behaviour is due to the densification of the microstructure of the concrete (28, 29) and

might mean a qualitative advance in the durability of the material, which would result in a significant increase of service life or a notable reduction of the coating thicknesses of reinforced structural elements in aggressive environments.

Other published works have identified relationships between the chloride migration coefficient and electrical resistivity (44, 48). Figure 8 shows the

potential correlation between these two parameters for the concretes after 28 days of curing. As may be observed, the potential correlation presents a good fit ($R^2 = 0.9576$).

3.4. Total, free and binding chloride concentration profiles

This section shows the results of chloride diffusion testing according to the CEN/TS 12390-11 standard (36), studying how the total amount of silica addition influences the penetration profile. Figures 9a, 9b, 9c, 10a, 10b, 10c, 11a, 11b and 11c show the profiles of total (a), free (b) and combined (c) chlorides of the concretes with a total addition of 2.5%, 5% and 7.5%, respectively, in comparison with the reference concrete, HAC.

Figure 9 shows that HAC[nSi]-2.5 and HAC[mSi]-2.5 have a similar total chloride penetration depth, significantly lower than the depth for

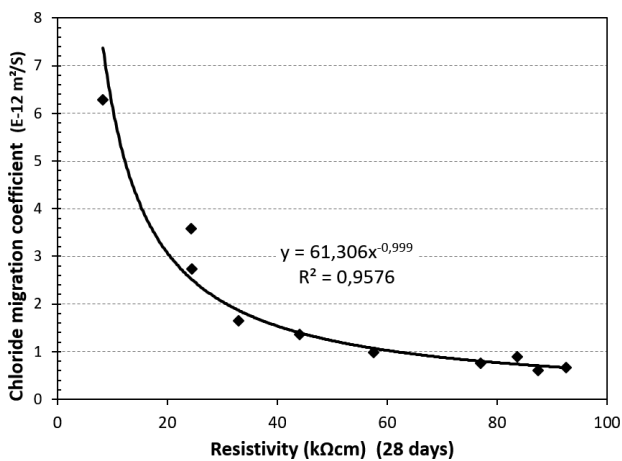


FIGURE 8. Correlation curves between the chloride migration coefficient and electrical resistivity.

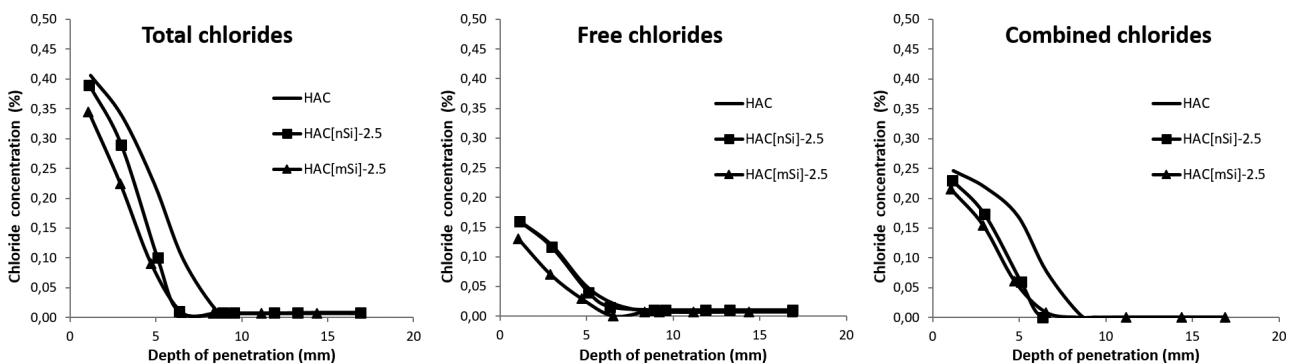


FIGURE 9. Chloride concentration profiles of the concretes with a total addition of 2.5% compared with HAC: a) total chlorides, b) free chlorides, c) combined chlorides.

HAC. However, concrete with nSi has an amount of free chlorides similar to that of HAC, though it has a notably lower amount of total chlorides, which means that the concentration of combined chlorides is lower than in the reference concrete. This figure shows that the addition of mSi leaves fewer free chlorides at the same depths, giving the concrete an increase in its chloride binding capacity.

The penetration profiles of the concretes with a total addition of 5% are shown in Figure 10, confirming the behaviour of the mSi. In this case, the amount of chlorides obtained with HAC[mSi]-5 and HAC[nmSi]-2.5/2.5 is similar. However, the percentage of free chlorides is lower for the case of binary concrete with mSi. The ternary mixture HAC[nmSi]-2.5/2.5 presented the second-lowest percentage of free chlorides and the lowest content of combined chlorides.

The case of the concretes with a total addition of 7.5% is shown in Figure 11. All cases presented similar profiles of total, free and combined chlorides and closely grouped depths of penetration. In this case, with 7.5% nSi the chloride binding capacity was close to the capacity with 7.5% mSi. Likewise, regardless of the combination of additions, the behaviour of these concretes was closely grouped. This means that, for this amount of total addition, the size of the addition does not significantly influence chloride penetration, which mainly depends on the activity of the silica.

3.5. Chloride diffusion coefficient

Figure 12, Figure 13 and Figure 14 show the chloride diffusion coefficient for mixtures with nSi, mixtures with mSi and ternary mixtures of nmSi, respectively, compared with HAC.

Figure 12 also shows a significant decrease in the chloride diffusion coefficient in comparison with the coefficient for the reference concrete, in a range from 46.78% with HAC[nSi]-2.5 to 83.58% with

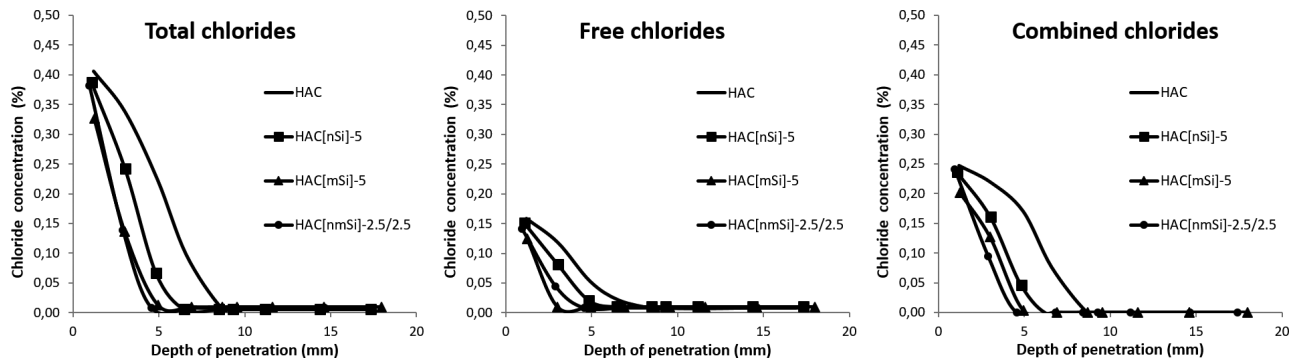


FIGURE 10. Chloride concentration profiles of the concretes with a total addition of 5% compared with HAC: a) total chlorides, b) free chlorides, c) combined chlorides.

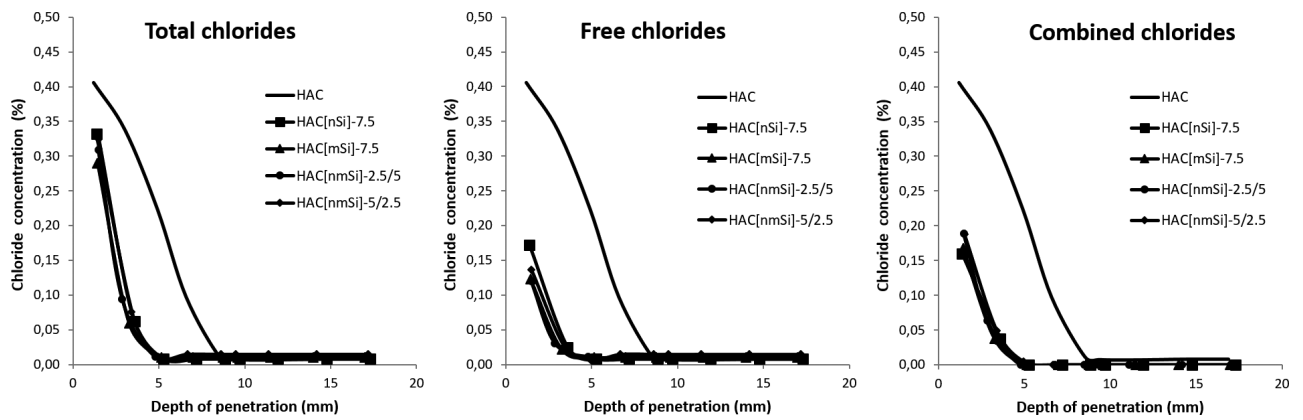


FIGURE 11. Chloride concentration profiles of the concretes with a total addition of 7.5% compared with HAC: a) total chlorides, b) free chlorides, c) combined chlorides.

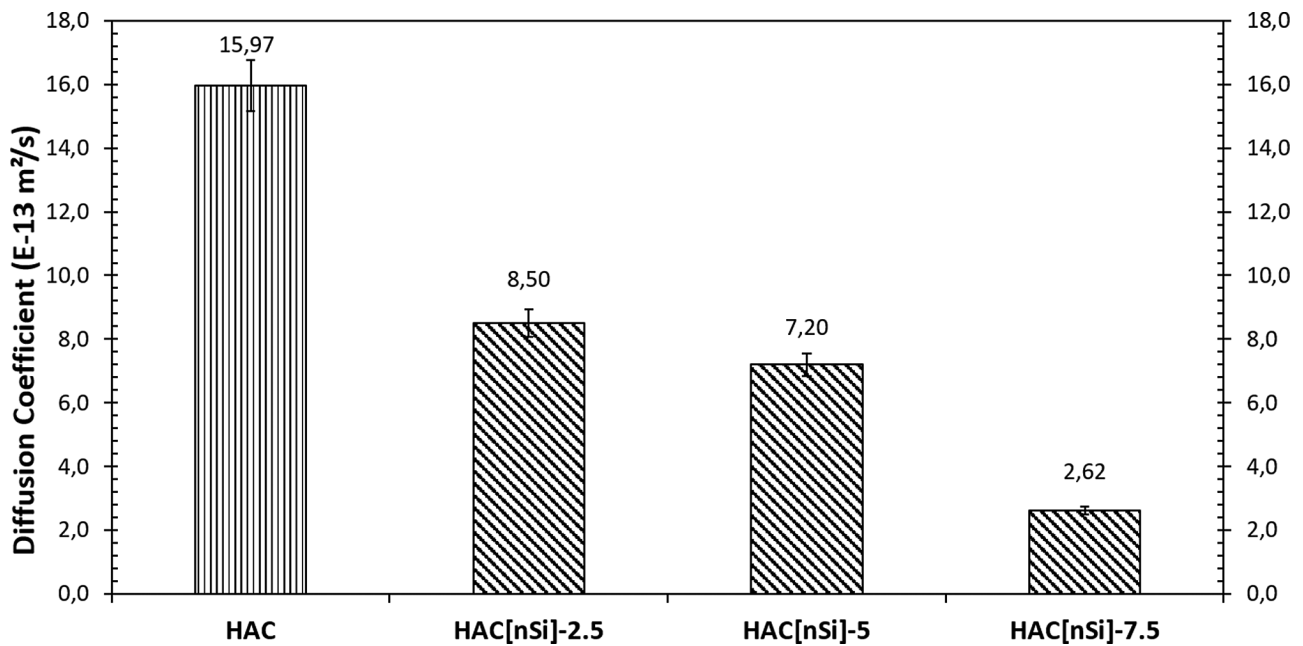


FIGURE 12. Chloride diffusion coefficient for mixtures with nSi compared with HAC.

HAC[nSi]-7.5. The chloride diffusion coefficient behaviour of these concretes is somewhat different from their chloride migration coefficient behaviour; when the amount of addition was increased from 2.5% to 5%, the decrease in the diffusion coefficient was only 8.12%, whereas the effect was much stronger in the case of the migration coefficient.

Figure 13 shows a similar trend in the case of binary concretes with nanosilica, although they exhibit a nearly linear decrease of their chloride diffusion coefficient with the percentage of addition. In this case, the percentages of decrease were 50.99% for HAC[mSi]-2.5, 75.54% for HAC[mSi]-5 and 86.09% for HAC[mSi]-7.5.

Figure 14 shows that for ternary mixtures the chloride diffusion coefficient was reduced by 78 to 87% in comparison with the value obtained for HAC. The concrete with the lowest diffusion coefficient is the same that presented the lowest chloride migration coefficient, HAC[nmSi]-5/2.5; it presented a value of $2.03 \times 10^{-13} \text{ m}^2/\text{s}$. The other ternary mixtures exhibited similar values: 3.43×10^{-13} for HAC[nmSi]-2.5/2.5 and $2.74 \times 10^{-13} \text{ m}^2/\text{s}$ for HAC[nmSi]-2.5/5.

The study of total, free and combined chloride penetration presented in the previous section might explain why the chloride diffusion coefficient is higher for binary concretes with nSi than for binary concretes with mSi when the percentage of addition is 2.5% or 5%. This might be caused by a greater chloride binding capacity provided by the addition of mSi to concrete. However, this trend changes

when the percentage of total addition is 7.5%. Then the concretes exhibit similar behaviour with comparable degrees of total, free and combined chloride concentration, as well as similar chloride diffusion coefficients. This could mean that the behaviour of 7.5% additions does not depend on silica size.

Figure 15 shows the correlation between the chloride diffusion coefficient and the chloride migration coefficient for the concretes studied.

The figure shows a linear relationship with a fairly good fit, $R^2 = 0.9571$, between the parameters. Therefore, given that the information provided by the migration test follows the same trend as that of the chloride diffusion test, such information could be used in studies of concrete behaviour with respect to chloride penetration. This is important due to the reduction in time, since use of the chloride migration test provides quantitative results in a maximum of five days, whereas with a natural diffusion test 90 days of exposure are necessary before proceeding to the chloride valuation to find the diffusion coefficient.

Figure 16 shows the potential correlation between resistivity and the chloride diffusion coefficient for the concretes studied. The fit is good ($R^2 = 0.9605$).

These accurate fits might allow relations to be established for inferring values, although the experimental campaign would have to be extended in order to validate the correlations in HPSCC with micro- and nanosilica additions.

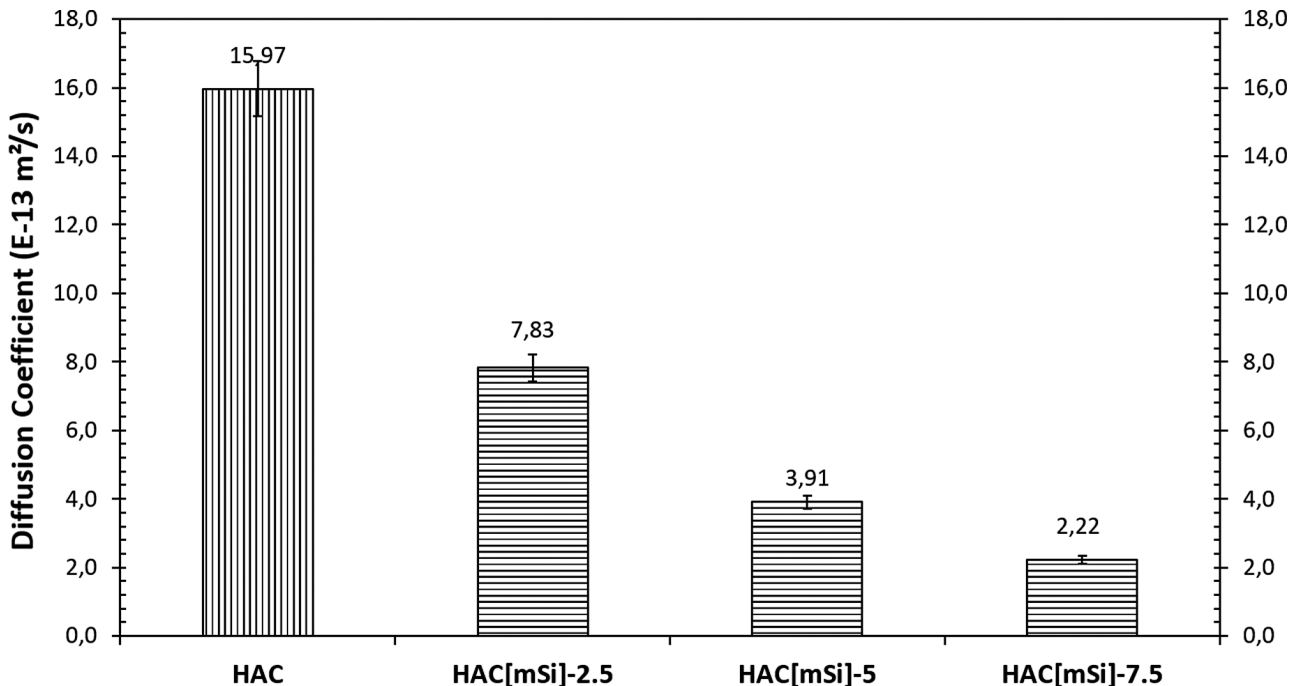


FIGURE 13. Chloride diffusion coefficient for mixtures with mSi compared with HAC.

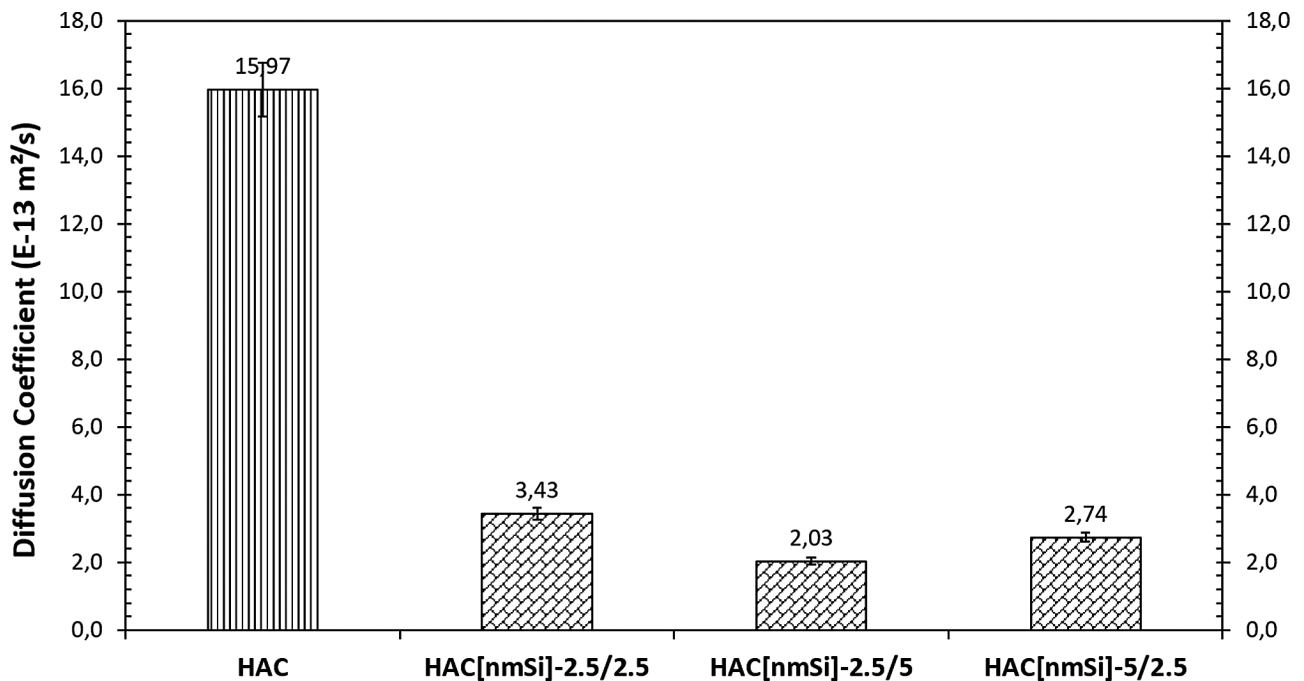


FIGURE 14. Chloride diffusion coefficient for mixtures of nmSi compared with HAC.

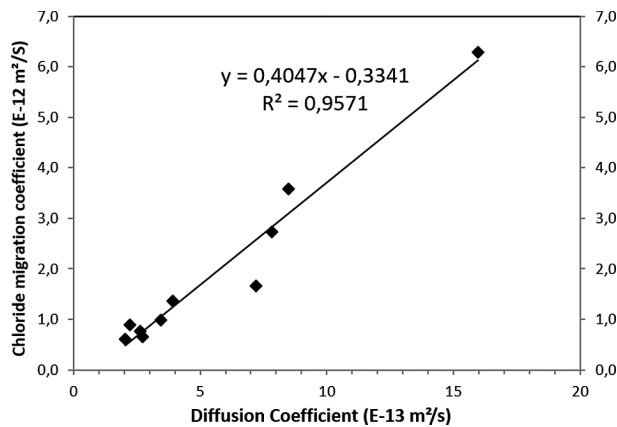


FIGURE 15. Correlation line between the chloride diffusion coefficient and the chloride migration coefficient for the mixtures.

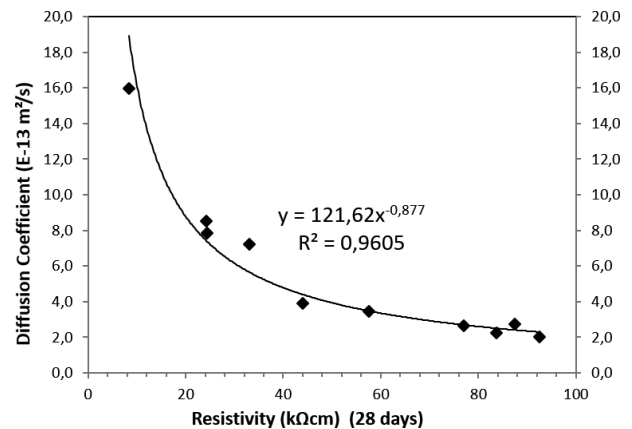


FIGURE 16. Correlation curve between resistivity and chloride diffusion coefficient for the mixtures.

Structure service life may be estimated using the model described in EHE 08 (13) and the chloride diffusion coefficient obtained by this study. The chloride penetration coefficient K_{Cl} is calculated by Equation [7]. The calculation assumes the worst-case values from EHE 08 (13): $C_{th} = 0.6\%$ and $C_s = 0.7\%$. From the K_{Cl} calculated, the depth of chloride penetration is obtained as a function of time and can be represented.

Figure 17 shows the estimated chloride penetration by natural diffusion as a function of time for the reference concrete and binary concretes

with nSi. As the amount of addition increases, the time to chloride penetration to the same depth increases, too. As a reference, a continuous line is represented at 20 mm of depth, so that the time taken to start corrosion with a coating of this thickness may be established. For HAC the corrosion initiation time is slightly greater than 100 years, while when only 2.5% nSi is added the estimated time is 219 years. This indicates that the use of nSi additions could reduce coating thickness while maintaining the service life established by regulations.

The estimated times of chloride penetration in binary concretes with mSi are shown in Figure 18. As in the case of nSi, the penetration time decreases as the amount of addition in the concrete increases. The corrosion initiation times for a coating of 20 mm range from 238 years for HAC[mSi]-2.5 to 839 years for HAC[mSi]-7.5.

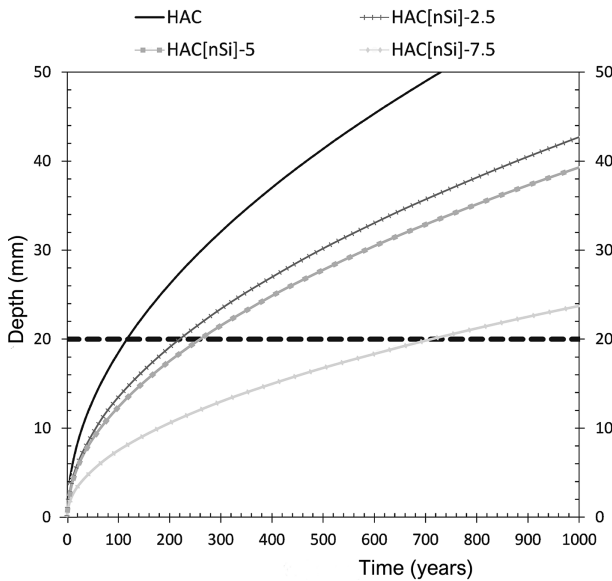


FIGURE 17. Estimated chloride penetration by natural diffusion as a function of time for the reference concrete and binary concretes with nSi.

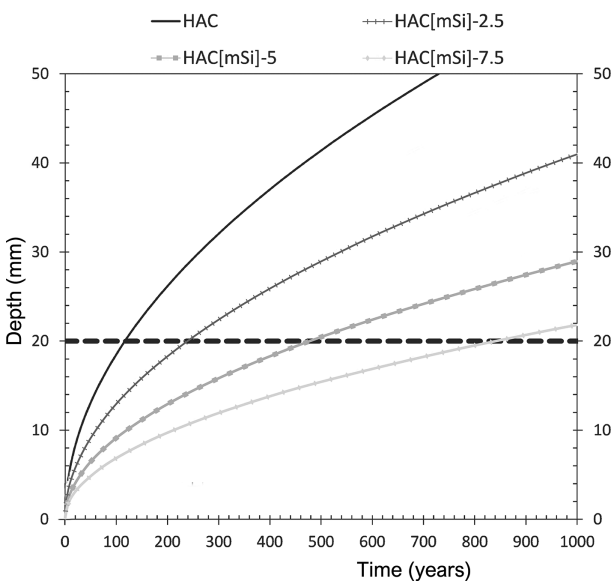


FIGURE 18. Estimated chloride penetration by natural diffusion as a function of time for the reference concrete and binary concretes with mSi.

Lastly, the estimate of chloride penetration for ternary concretes is shown in Figure 19. In this type of concrete, HAC[nmSi]-5/2.5 presented the best chloride resistance, as might be expected from the diffusion coefficient results. The corrosion initiation time for a coating of 20 mm is 543 years for HAC[nmSi]-2.5/2.5, 918 years for HAC[nmSi]-5/2.5 and 681 years for HAC[nmSi]-2.5/5.

Table 7 shows the estimated corrosion initiation time for a structural element coating of 20 mm of each concrete studied, listed according to the total addition.

Adding 2.5% nano- or microsilica yields similar estimated corrosion initiation times regardless of the size of the addition. Both additions double the corrosion initiation time for HAC, although microsilica provides a slightly higher value.

In the case of concretes with a total addition of 5%, the estimated corrosion initiation time for binary concrete with mSi is 85% higher than that of binary concrete with nSi. This might be due to the difficulty of compaction of mixtures with a high nSi content. However, the longest corrosion initiation time is obtained with the ternary mixture, probably due to a packing effect and the low porosity created by a wider particle size distribution (29).

HAC[nmSi]-5/2.5 has the longest estimated service life of all the mixtures featuring a total addition of 7.5%. This mixture represents the best combination of nano- and microsilica addition for resisting chloride penetration, probably due to the optimisation of the packing effect, overcoming the difficulties in compaction caused by considerable percentages of nSi.

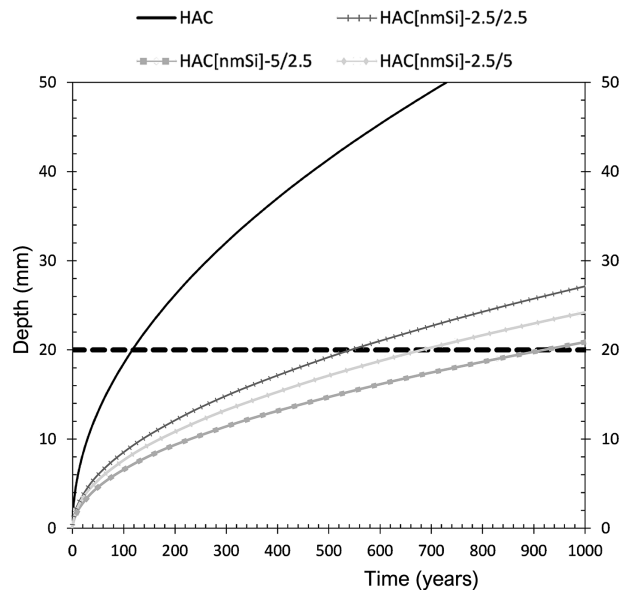


FIGURE 19. Estimated chloride penetration by natural diffusion as a function of time for the reference concrete and ternary concretes with nmSi.

The experimental results and the estimated service life may be interpreted by taking into account that nano- and microsilica additions reduce the amount of interconnected pores, since their incorporation in cement blends leads to a refinement of the porous network and changes the ionic concentration in the pore solution (49, 50). These additions combine pozzolanic action, which increases the amount of C-S-H gels, with the filling effect, as the small size of the addition particles blocks small pores and prevents their interconnection.

The results shown in Table 7 indicate that ternary mixtures might be the best for improving the durable properties of concrete, since in the worst case their estimated service life ranges from over five times higher to over eight times higher than that of HAC. This could be explained by considering that in ternary mixtures pores are filled more efficiently, causing them to reduce interconnection to a greater extent, as the particle size continuity is greater (29).

Additionally, ternary mixtures show good self-compacting properties (see Table 3) while demanding a lower SP content than nSi binary mixtures that contain the same total amount of additions, and they do not present the same handling difficulties as blends with nS alone. Furthermore, these mixtures present the best mechanical behaviour.

4. CONCLUSIONS

HPSCC with the addition of nano- and microsilica in binary and ternary mixtures presents significant improvements in chloride-resistant behaviour. This improvement is in general proportional to the total content of addition. The use of nSi and mSi may have a positive effect on improving the microstructure and reducing the internal pore structure from early stages.

In binary mixtures the addition of microsilica presents higher values of electrical resistivity than

the addition of nanosilica. However, when classified by resistivity, all mixtures, both binary and ternary, exhibit a notably low chloride penetrability.

Similarly, binary mixtures prepared with microsilica exhibit lower chloride migration coefficients than binary mixtures with nanosilica. Significantly lower values are obtained with ternary mixtures, however, even in the case of the mixture with the smallest amount of each addition.

The addition of microsilica provides the concrete with a greater capacity for chloride combination than does the addition of nanosilica for percentages less than or equal to 5%.

Binary mixtures prepared with microsilica have lower chloride diffusion coefficients than binary mixtures with nanosilica at 28 days. However, the combination of both additions in ternary mixtures results in significantly low chloride diffusion coefficients, even at small addition ratios. Further future study including additional parameters, such as chloride diffusion coefficients at different ages, is necessary in order to examine the influence of nSi and mSi on the durability of concrete mixtures, in particular at early ages, where the microstructure improvements obtained are promising.

The chloride diffusion coefficients and the concentrations of total, free and combined chlorides were similar in each concrete containing a total addition of 7.5%, regardless of the amount of silica addition.

The addition of nano- and microsilica in binary and ternary mixtures leads to notably low chloride diffusion coefficients, with a significant increase in the estimated service life according to Spanish regulations. These results might also allow the thickness of cover to reinforcement to be reduced without leading to negative consequences for structure durability.

ACKNOWLEDGEMENTS

The authors wish to express their gratitude to the Spanish Ministry of Science and Innovation (Ministerio de Ciencia e Innovación), project RTI2018-100962-B-I00, for financial support.

REFERENCES

1. Siddique, R. (2013) Compressive strength, water absorption, sorptivity, abrasion resistance and permeability of self-compacting concrete containing coal bottom ash. *Construc. Build. Mat.* 47, 1444–1450. <https://doi.org/10.1016/j.conbuildmat.2013.06.081>.
2. Łązniewska-Piekarczyk, B. (2014) The methodology for assessing the impact of new generation superplasticizers on air content in self-compacting concrete. *Construc. Build. Mat.* 53, 488–502. <https://doi.org/10.1016/j.conbuildmat.2013.11.092>.
3. Mohammed, M.K.; Dawson, A.R.; Thom, N.H. (2014) Carbonation of filler typed self-compacting concrete and its impact on the microstructure by utilization of 100% CO₂

TABLE 7. Estimated corrosion initiation time for a 20-mm coating.

Amount of addition	Concrete	Corrosion initiation time (years)	Increase with respect to HAC (years)
0	HAC	116.72	0
2.5	HAC[nSi]-2.5	219.31	102.59
2.5	HAC[mSi]-2.5	238.13	121.41
5	HAC[nSi]-5	258.79	142.07
5	HAC[mSi]-5	477.22	360.49
5	HAC[nmSi]-2.5/2.5	543.01	426.29
7.5	HAC[nSi]-7.5	710.88	594.15
7.5	HAC[mSi]-7.5	839.01	722.29
7.5	HAC[nmSi]-5/2.5	918.46	801.74
7.5	HAC[nmSi]-2.5/5	681.36	564.64

- accelerating techniques. *Construc. Build. Mat.* 50, 508–516. <https://doi.org/10.1016/j.conbuildmat.2013.09.052>.
4. Druta, C.; Wang, L.; Lane, D.S. (2014) Tensile strength and paste-aggregate bonding characteristics of self-consolidating concrete. *Construc. Build. Mat.* 55, 89–96. <https://doi.org/10.1016/j.conbuildmat.2014.01.010>.
 5. Jalal, M.; Pouladkhan, A.; Harandi, O.F.; Jafari, D. (2015) Comparative study on effects of Class F fly ash, nano silica and silica fume on properties of high performance self-compacting concrete. *Construc. Build. Mat.* 94, 90–104. <https://doi.org/10.1016/j.conbuildmat.2015.07.001>.
 6. Güneysi, E.; Gesoglu, M.; Al-Goody, A.; Ipek, S. (2015) Fresh and rheological behavior of nano-silica and fly ash blended self-compacting concrete. *Construc. Build. Mat.* 95, 29–44. <https://doi.org/10.1016/j.conbuildmat.2015.07.142>.
 7. Hemalatha, T.; Ram Sundar, K.R.; Ramachandra Murthy, A.; Iyer, N. R. (2015) Influence of mixing protocol on fresh and hardened properties of self-compacting concrete. *Construc. Build. Mat.* 98, 119–127. <https://doi.org/10.1016/j.conbuildmat.2015.08.072>.
 8. Puentes, J.; Barluenga, G.; Palomar, I. (2015) Effect of silica-based nano and micro additions on SCC at early age and on hardened porosity and permeability. *Construc. Build. Mat.* 81, 154–161. <https://doi.org/10.1016/j.conbuildmat.2015.02.053>.
 9. Leung, H.Y.; Kim, J.; Nadeem, A.; Jaganathan, J.; Anwar, M.P. (2016) Sorptivity of self-compacting concrete containing fly ash and silica fume. *Construc. Build. Mat.* 113, 369–375. <https://doi.org/10.1016/j.conbuildmat.2016.03.071>.
 10. Tian, J.; Wang, W.; Du, Y. (2016) Damage behaviors of self-compacting concrete and prediction model under coupling effect of salt freeze-thaw and flexural load. *Construc. Build. Mat.* 119, 241–250. <https://doi.org/10.1016/j.conbuildmat.2016.05.073>.
 11. Asadollahi, S.; Saeedian, A.; Dehestani, M.; Zahedi, F. (2016) Improved compressive fracture models for self-consolidating concrete (SCC). *Construc. Build. Mat.* 123, 473–480. <https://doi.org/10.1016/j.conbuildmat.2016.07.030>.
 12. Specification and Guidelines for Self-Compacting Concrete. (2005) European Federation for Specialist Construction Chemicals and Concrete Systems EFNARC.
 13. Instrucción de Hormigón Estructural (EHE). (2010) Ministerio de Fomento, Secretaría General Técnica, Madrid.
 14. Nepomuceno, M.C.S.; Oliveira, L.A.; Lopes, S.M.R. (2014) Methodology for mix design of self-compacting concrete using different mineral additions in binary blends of powders. *Construc. Build. Mat.* 26, 317–326. <https://doi.org/10.1016/j.conbuildmat.2011.06.027>.
 15. Shi, C.; Wu, Z.; Lv, K.; Wu, L. (2015) A review on mixture design methods for self-compacting concrete. *Construc. Build. Mat.* 84, 387–398. <https://doi.org/10.1016/j.conbuildmat.2015.03.079>.
 16. Ye, G.; Liu, X.; De Schutter, G.; Poppe, A.-M.; Taerwe, L. (2007) Influence of limestone powder used as filler in SCC on hydration and microstructure of cement pastes. *Cem. Concr. Compos.* 29, 94–102. <https://doi.org/10.1016/j.cemconcomp.2006.09.003>.
 17. Barluenga, G.; Palomar, I.; Puentes, J. (2015) Hardened properties and microstructure of SCC with mineral additions. *Construc. Build. Mat.* 94, 728–736. <https://doi.org/10.1016/j.conbuildmat.2015.07.072>.
 18. Jalal, M.; Pouladkhan, A.; Harandi, O.F.; Jafari, D. (2015) Comparative study on effects of Class F fly ash, nano silica and silica fume on properties of high performance self-compacting concrete. *Construc. Build. Mat.* 94, 90–104. <https://doi.org/10.1016/j.conbuildmat.2015.07.001>.
 19. Owsiak, Z.; Grzmil, W. (2015) The evaluation of the influence of mineral additives on the durability of self-compacting concretes. *KSCE J. Civil Engineer.* 19, 1002–1008. <https://doi.org/10.1007/s12205-013-0336-7>.
 20. Ghafari, E.; Costa, H.; Júlio, E.; Portugal, A.; Durães, L. (2014) The effect of nanosilica addition on flowability, strength and transport properties of ultra-high performance concrete. *Mater. Design.* 59, 1–9. <https://doi.org/10.1016/j.matdes.2014.02.051>.
 21. Li, Z.; Peng, J.; Ma, B. (1999) Investigation of chloride diffusion for high-performance concrete containing fly ash, microsilica and chemical admixtures. *ACT Mater. J.* 96, 391–396.
 22. Björnstrom, J.; Martinelli, A.; Matic, A.; Börjesson, L.; Panas, I. (2004) Accelerating effects of colloidal nano-silica for beneficial calcium-silica-hydrate formation in cement. *Chem. Phys. Lett.* 392 [1–3], 242–248. <https://doi.org/10.1016/j.cplett.2004.05.071>.
 23. Jo, B-W.; Kim, C-H.; Tae, G-H.; Park, J-B. (2007) Characteristics of cement mortar with nano-SiO₂ particles. *Construc. Build. Mat.* 21, 1351–1355. <https://doi.org/10.1016/j.conbuildmat.2005.12.020>.
 24. Kawashima, S.; Hou, P.; Corr, D.J.; Shah, S.P. (2013) Modification of cement-based materials with nanoparticles. *Cem. Concr. Compos.* 36, 8–15. <https://doi.org/10.1016/j.cemconcomp.2012.06.012>.
 25. Rong, Z.; Sun, W.; Xiao, H.; Jiang, G. (2015) Effects of nano-SiO₂ particles on the mechanical and microstructural properties of ultra-high performance cementitious composites. *Cem. Concr. Compos.* 56, 25–31. <https://doi.org/10.1016/j.cemconcomp.2014.11.001>.
 26. Balapour, M.; Joshaghani, A.; Althoey, F. (2018) Nano-SiO₂ contribution to mechanical, durability, fresh and microstructural characteristics of concrete: A review. *Construc. Build. Mat.* 181, 27–41. <https://doi.org/10.1016/j.conbuildmat.2018.05.266>.
 27. Gesoglu, M.; Güneysi, E.; Asaad, D.S.; Muhyaddin, G.F. (2016) Properties of low binder ultra-high performance cementitious composites: Comparison of nanosilica and microsilica. *Construc. Build. Mat.* 102, 706–713. <https://doi.org/10.1016/j.conbuildmat.2015.11.020>.
 28. Bernal, J.; Reyes, E.; Massana, J.; León, N.; Sánchez, E. (2018) Fresh and mechanical behavior of a self-compacting concrete with additions of nano-silica, silica fume and ternary mixtures. *Construc. Build. Mat.* 160, 196–210. <https://doi.org/10.1016/j.conbuildmat.2017.11.048>.
 29. Massana, J.; Reyes, E.; Bernal, J.; León, N.; Sánchez-Espinosa, E. (2018) Influence of nano- and micro-silica additions on the durability of a high-performance self-compacting concrete. *Construc. Build. Mat.* 165, 93–103. <https://doi.org/10.1016/j.conbuildmat.2017.12.100>.
 30. Ryan, P.C.; O'Connor, A. (2016) Comparing the durability of self-compacting concretes and conventionally vibrated concretes in chloride rich environments. *Construc. Build. Mat.* 120, 504–513. <https://doi.org/10.1016/j.conbuildmat.2016.04.089>.
 31. UNE-EN 197-1:2011 Cement - Part 1: Composition, specifications and conformity criteria for common cements. Asociación Española de Normalización y Certificación AENOR. www.aenor.es.
 32. UNE 12620:2003+A1:2009 Aggregates for concrete. Asociación Española de Normalización y Certificación, AENOR. www.aenor.es.
 33. UNE 83988-1:2008 Concrete durability. Test methods. Determination of the electrical resistivity. Part 1: Direct test (reference method), Asociación Española de Normalización y Certificación AENOR. www.aenor.es.
 34. ASTM C1202-18 (2018) Standard Test Method for Electrical Indication of Concrete's Ability to Resist Chloride Ion Penetration. ASTM International.
 35. NT BUILD 492 (1999) Concrete, mortar and cement-based repair materials: Chloride migration coefficient from non-steady-state migration experiments. Nordtest. ISSN 0283–7153.
 36. CEN/TS 12390-11:2010 Testing hardened concrete - Part 11: Determination of the chloride resistance of concrete, unidirectional diffusion. European Committee for Standardization.
 37. UNE-EN 14629:2007 Products and systems for the protection and repair of concrete structures - Test methods - Determination of chloride content in hardened concrete, Asociación Española de Normalización y Certificación, AENOR. <http://www.aenor.es>.

38. RILEM Publications. (2002). Analysis of total chloride content in concrete. *Mater. Struct.* 35, 583–585. <https://doi.org/10.1007/BF02483128>.
39. Sing, K.S.W.; Everett, D.H.; Haul, R.A.W.; Moscou, L.; Pierotti, R.A.; Rouquerol, J.; et al. (1985) IUPAC (Recommendations 1984), Reporting physisorption data for gas/solid systems with special reference to the determination of surface area and porosity. *Pure Appl. Chem.* 57, 603–619. <https://doi.org/10.1351/pac198557040603>.
40. Polder, R.B. (2001) Test methods for on-site measurement of resistivity of concrete. RILEM TC-154 technical recommendation. *Constr. Build. Mater.* 15, 125–131. [https://doi.org/10.1016/S0950-0618\(00\)00061-1](https://doi.org/10.1016/S0950-0618(00)00061-1).
41. Basheer, P.; Gilleece, P.; Long, A.; Mc Carter, W. (2002) Monitoring electrical resistance of concretes containing alternative cementitious materials to assess their resistance to chloride penetration. *Cem. Concr. Compos.* 24, 437–449. [https://doi.org/10.1016/S0958-9465\(01\)00075-0](https://doi.org/10.1016/S0958-9465(01)00075-0).
42. Rajabipour, F.; Weiss, J.; Shane, J.D.; Mason, T.O.; Shah, S.P. (2005) Procedure to interpret electrical conductivity measurements in cover concrete during rewetting. *J. Mater. Civ. Eng.* 17, 586–594. [https://doi.org/10.1061/\(ASCE\)0899-1561\(2005\)17:5\(586\)](https://doi.org/10.1061/(ASCE)0899-1561(2005)17:5(586)).
43. McPolin, D.; Basheer, P.A.M.; Long, A.E.; Grattan, K.T.V.; Sun, T. (2005) Obtaining progressive chloride profiles in cementitious materials. *Constr. Build. Mater.* 19, 666–673. <https://doi.org/10.1016/j.conbuildmat.2005.02.015>.
44. Andrade, C.; D'Andrea, R.; Rebolledo, N. (2014) Chloride ion penetration in concrete: the reaction factor in the electrical resistivity model. *Cem. Concr. Compos.* 47, 41–46. <https://doi.org/10.1016/j.cemconcomp.2013.09.022>.
45. Romero Mendoza, H.R. (2011) Deterioro del hormigón sometido a ensayos acelerados de hielo-deshielo en presencia de cloruros, PhD dissertation, Escuela Técnica Superior de Ingeniería de Caminos, Canales y Puertos, Universidad Politécnica de Madrid, Madrid, Spain.
46. Jalal, M.; Mansouri, E.; Sharifipour, M.; Pouladkhan, A.R. (2012) Mechanical, rheological, durability and microstructural properties of high performance self-compacting concrete containing SiO₂ micro and nanoparticles. *Mater. Design.* 34, 389–400. <https://doi.org/10.1016/j.matdes.2011.08.037>.
47. Li, L.G.; Zhu, J.; Huang, Z.H.; Kwan, A.K.H.; Li, L.J. (2017) Combined effects of micro-silica and nano-silica on durability of mortar. *Construc. Build. Mat.* 157, 337–347. <https://doi.org/10.1016/j.conbuildmat.2017.09.105>.
48. Zahedi, M.; Ramezaniapour, A.A.; Ramezaniapour, A.M. (2015) Evaluation of the mechanical properties and durability of cement mortars containing nanosilica and rice husk ash under chloride ion penetration. *Construc. Build. Mat.* 78, 354–361. <https://doi.org/10.1016/j.conbuildmat.2015.01.045>.
49. Alonso-Domínguez, D.; Álvarez-Serrano, I.; Reyes, E.; Moragues, A. (2017) New mortars fabricated by electrostatic dry deposition of nano and microsilica additions: Enhanced properties. *Construc. Build. Mat.* 135, 186–193. <https://doi.org/10.1016/j.conbuildmat.2017.01.011>.
50. Olsson, N.; Lothenbach, B.; Baroghel-Bouny, V.; Nilsson, L-O. (2018) Unsaturated ion diffusion in cementitious materials – The effect of slag and silica fume. *Construc. Build. Mat.* 108, 31–37. <https://doi.org/10.1016/j.cemconres.2018.03.007>.